Mon. Not. R. Astron. Soc. **000**, 000–000 (0000) Printed 6 September 2016 (MN LATEX style file v2.2)

FIGGS2: An HI survey of extremely faint irregular galaxies

Narendra Nath Patra[1] ⋆, Jayaram N. Chengalur[1] †, Igor D. Karachentsev[2] ‡, Margarita E. Sharina[2]
[1] *NCRA-TIFR, Post Bag 3, Ganeshkhind, Pune 411 007, India*
[2] *Special Astrophysical Observatory, Nizhnij Arkhyz, Karachai-Cherkessia 369167, Russia*

arXiv:1609.01072v1 [astro-ph.GA] 5 Sep 2016

ABSTRACT

We present the observations and first results from the FIGGS2 survey. FIGGS2 is an extension of the earlier Faint Irregular Galaxies GMRT survey (FIGGS) towards faint luminosity end. The sample consists of 20 galaxies of which 15 were detected in HI 21cm line using the Giant Meter-wave Radio Telescope (GMRT). The median blue band magnitude of our sample is ~ -11.6, which is more than one magnitude fainter than earlier FIGGS survey. From our GMRT observations we find that, for many of our sample galaxies, the HI disks are offset from their optical disks. The HI diameters of the FIGGS2 galaxies show a tight correlation with their HI mass. The slope of the correlation is 2.08 ± 0.20 similar to what is found for FIGGS galaxies. We also find that for almost all galaxies, the HI disks are larger than the optical disks which is a common trend for dwarf or spiral galaxies. The mean value of the ratio of HI to optical diameter is ~ 1.54.

Key words: galaxies: dwarf - galaxies: evolution - galaxies: ISM

1 INTRODUCTION

There are a number of issues that make systematic studies of dIrr galaxies particularly interesting. Firstly, in hierarchical models of galaxy formation, small objects form first and merge together to form larger objects. In that sense, nearby dwarf galaxies are the closest analogues to the galaxies in the early universe. Secondly, the ISM of dwarf galaxies have low metallicity. In this sense too, they are analogous to high redshift galaxies, and serve as a nearby laboratory for the study of gas and star formation in environments with low dust and low metallicity (Roychowdhury et al. 2009, 2011). This is in part responsible for the increasing number of recent surveys of dwarf galaxies, e.g. FIGGS (Begum et al. 2008), SHIELD (Cannon et al. 2011), VLA-ANGST (Ott et al. 2012), LITTLE-THINGS (Hunter et al. 2012).

In this paper we describe an extension to the FIGGS (Begum et al. 2008) survey. This extension focuses on galaxies with fainter luminosities and smaller HI masses. We present here the results of our HI observations of 20 very faint galaxies with the Giant Meterwave Radio Telescope (GMRT). In §2 we describe our sample, in §3 we explain the main science drivers of the survey, in §4 we present the observations and data analysis and finally in §5 we present the results and discussion.

⋆ E-mail: narendra@ncra.tifr.res.in
† E-mail: chengalu@ncra.tifr.res.in
‡ E-mail: ikar@sao.ru

2 SAMPLE

The FIGGS2 survey was planned as an extension of the Faint Irregular Galaxy GMRT Survey (FIGGS) (Begum et al. 2008). The FIGGS sample was based on the 2004 version of a compilation of nearby galaxies (Catalogue of Nearby Galaxies (Karachentsev et al. 2004)). Since then there has been an almost two fold increase in the known number of faint galaxies in the local neighbourhood, thanks to surveys like the SDSS (Abazajian et al. 2009) and ALFALFA (Giovanelli et al. 2005). In the FIGGS2 survey we focus on the faintest end of the galaxy spectrum, viz. galaxies with $\mathrm{M_B} \gtrsim -12$. The cutoff magnitude for the FIGGS sample was $\mathrm{M_B} = -14.5$ and the sample contained $\sim$ 11 galaxies fainter than $\mathrm{M_B} = -12$. The FIGGS2 sample consists of 20 galaxies with $\mathrm{M_B} \gtrsim -12.0$, and $S_{\mathrm{HI}} \gtrsim 0.5$ Jy km/s which combined with FIGGS galaxies leads to a $\sim$ 3 times larger sample of galaxies fainter than $\mathrm{M_B} = -12.0$ than was earlier available. We note that revision to the distance and other observable parameters have resulted in two of our galaxies now having $\mathrm{M_B}$ slightly larger than -12. The galaxies were selected from the Updated Nearby Galaxy Catalog (UNGC) (Karachentsev et al. 2004) as per the telescope scheduling constraints. FIGGS sample consists of 66 galaxies out of $\sim$ 230 galaxies in the UNGC catalog satisfying selection criteria of FIGGS, whereas, 15 galaxies were observed with the GMRT as part of FIGGS2, out of $\sim$ 85 galaxies in NGC catalogue which satisfy selection criteria of FIGGS2. Most of the remaining objects (unobserved within FIGGS+FIGGS2) reside on the southern sky bellow the GMRT horizon.

In Table 1 we list a few general properties of our sample galax-

ies. The columns are as follows: column (1): Galaxy name, column (2) and (3): the equatorial coordinates (J2000), column (4): Distance in Mpc, column (5): the methods used to determine the distances to the galaxies, - by the tip of the red giant branch (TRGB), by the Hubble velocity-distance relation (H_0 = 73 km/s/Mpc) (h), from galaxy membership (mem), column (6) the absolute blue magnitude (extinction corrected), column (7): log of HI mass, column (8) Heliocentric radial velocity, column (9): The Holmberg diameter, column (10): inclination derived from optical photometry (assuming an intrinsic thickness of 0.42 (Roychowdhury et al. 2013)). The data presented in Table 1 were taken from (Karachentsev et al. 2013, 2001; Makarov et al. 2003; Huchtmeier et al. 2000, 2009). The first 15 galaxies in Table 1 were detected in our GMRT observations, whereas the last five galaxies (separated by an empty line) were not detected.

In Figure 1 we plot histograms of various global properties of our sample galaxies. To compare our survey with other major surveys, we plot histograms of sample galaxy properties of two major surveys of dwarf galaxies namely, the LITTLE-THINGS survey (Hunter et al. 2012) and the VLA-ANGST survey (Ott et al. 2012). The solid black histograms in Fig. 1 represents FIGGS2 survey data, whereas the blue dashed-dotted and the red dashed histograms represent the LITTLE-THINGS and the VLA-ANGST data respectively. In panel [A] we plot the histograms of absolute blue magnitude $\mathrm{M_B}$, panel [B] shows the histograms of $\log$ of HI mass, panel [C] and [D] shows the histograms of distances to the sample galaxies and the HI mass to blue luminosity ratio ($\mathrm{M_{HI}/L_B}$) respectively. Since the distances to some of our galaxies have been updated after the sample selection was done, the estimated luminosities of some of our sample galaxies are brighter than the sample selection cut-off of $\mathrm{M_B} \gtrsim -12.0$. Nonetheless, the median $\mathrm{M_B}$ of the sample is -11.6, which is more than one magnitude fainter than the median of the FIGGS sample. Panel [B] (solid black line) shows the histogram of $\log$ of HI mass of our sample galaxies. The median HI mass of our sample galaxies is $\sim 8 \times 10^6$ $\mathrm{M_\odot}$ which is also about an order of magnitude lower than the median HI mass of FIGGS sample. From Figure 1 one can see that our sample spans $\sim$ 3 magnitude in brightness (a factor of $\sim$ 12) and $\sim$ 2 orders of magnitude in HI mass. We also note that our sample galaxies are concentrated around the low luminosity tail of the LITTLE-THINGS or the VLA-ANGST survey.

3 SCIENCE DRIVERS FOR FIGGS2

The primary goal of the FIGGS2 survey was to extend the previous FIGGS survey towards the fainter end and enrich the multi wave length data base to address several science questions. A few of the science drivers of FIGGS2 are discussed below.

Much of what we know about gas in the high redshift universe comes from the study of absorption line systems seen in front of bright quasars, i.e. the so called Damped Lyman-α absorption systems (DLAs). Although such studies allow one to inventory the total amount of atomic gas as a function of redshift, because the information received is limited to that along the pencil beam illuminated by the quasar, the nature of the host population of these systems remains unclear. An interesting question is as to whether their properties resemble that of the local dwarf galaxy population. One quantitative way of checking this is is to use data from surveys like the FIGGS and FIGGS2 surveys to see whether the column density distribution function of DLAs matches that observed in local dwarf galaxies (e.g. Patra et al. 2013).

The neutral ISM and its connection with the star-formation in gas-rich dwarf irregular galaxies has been a major area of interest for a long time. Star formation in these low dust, low metallicity environments is expected to proceed differently than in spiral galaxies. Though a number of studies using FIGGS data have already explored many aspects of star formation (see for example, Roychowdhury et al. 2009, 2011), yet a number of interesting questions still remain to be answered; like star formation feedback and its effect on star-formation in smallest scales, abundance of the different ISM phases and its connection with star formation etc. Very often the total measured Hα emission in these galaxies can be accounted for by only a few massive stars. Due to very shallow potential well of these galaxies, the ISM and cold gas are expected to be strongly affected by star formation feedback. A comparison of the HI and optical morphologies could allow one to examine the consequences of this feedback in the smallest gas-rich galaxies.

Another area of interest is in the phase structure of the atomic gas in these galaxies. In our own galaxy the atomic ISM is believed to have two stable phases that co-exist in pressure equilibrium, i.e. a dense cold phase (the Cold Neutral Medium) and a warm diffuse phase (the Warm Neutral Medium). There is also increasing evidence that a significant fraction of atomic gas is a phase with intermediate temperature, which would be thermally unstable. There have been several studies aimed at trying to understand the phase structure of the atomic gas in dwarf galaxies, and one would like to extend such studies to the smallest star forming units known. A related question would be as to what the connections, if any, are between the CNM phase and star formation in dwarf galaxies (e.g. (Patra et al. 2016)).

Another area of interest is to the structure of the dark matter halo and its influence on the structure and dynamics of dwarf galaxies (Banerjee and Jog 2008; Banerjee et al. 2010; Saha and Maciejewski 2013). The vertical structure and scale-height of galaxies is determined by the hydrostatic equilibrium between different galactic components (e.g. Narayan and Jog 2002) embedded in the dark matter halo. This vertical hydrostatic equilibrium decides in turn the thickness and the vertical structure of the galactic disk. Observationally it is found that the gas disks of small gas-rich galaxies (like our sample) are thicker than normal spirals (Roychowdhury et al. 2010). However a complete theoretical understanding of this higher thickness and the vertical structure of the gas disc of dwarf galaxies is not yet available. Similarly the presence of non-axi-sysmmetric structures also has implications for the dark matter distribution (Banerjee et al. 2013). One of the aims of this survey is to provide data for studies vertical structure of gas disks, which in turn can be used to constrain the distribution of the dark matter and the gas velocity dispersion (Patra et al. 2014).

4 OBSERVATION & DATA ANALYSIS

For all our observations we used the newly installed GMRT Software Back-end (GSB). A bandwidth of 2.08 MHz with 256 channels or a bandwidth of 4.17 MHz with 512 channels were used keeping the spectral resolution constant at $\sim$ 8.1 KHz (velocity width of $\sim$ 1.7 km $\mathrm{s^{-1}}$). In every observing run flux calibration and bandpass calibration were done by observing standard flux calibrators 3C48, 3C147 or 3C286 at the starting and at the end of the observation. The phase calibration were done by observing a phase calibrator from the VLA list of calibrators within an angular distance of $\lesssim$ 10^o of the source once in every 45 minutes.

Typically about 6 hrs of time was alloted for a single obser-

Table 1. Sample galaxy properties

Galaxy	α (J2000) (hhmmsss)	δ (J2000) (^{o} $'$ $''$)	Distance (Mpc)	Method	M_B (mag)	$\log M_{HI}$ ($M_\odot$)	V_{hel} km s^{-1}	D_{opt} (arcmin)	i_{opt} (^{o})
(1)	(2)	(3)	(4)	(5)	(6)	(7)	(8)	(9)	(10)
AGC112521	014107.9	+271926	6.08	$TRGB$	−11.4	6.75	274	0.60	67
KK15	014641.6	+264805	8.67	$TRGB$	−11.8	7.21	366	0.59	90
KKH37	064745.8	+800726	3.44	$TRGB$	−11.6	6.71	11	1.15	55
KKH46	090836.6	+051732	6.70	TF	−12.3	7.44	598	0.60	34
UGC04879	091602.2	+525024	1.36	$TRGB$	−11.9	5.98	-25	3.24	66
LeG06	103955.7	+135428	10.40	mem	−11.9	6.85	1007	0.63	57
KDG073	105257.1	+693245	3.91	$TRGB$	−10.9	6.56	116	1.20	38
VCC0381	121954.1	+063957	4.71	h	−11.7	7.14	480	0.78	26
KK141	122252.7	+334943	7.78	h	−11.5	7.20	573	0.40	45
KK152	123324.9	+332105	6.90	TF	−13.0	7.54	838	1.07	83
UGCA292	123840.0	+324600	3.85	$TRGB$	−11.9	7.49	308	1.02	52
BTS146	124002.1	+380002	8.50	TF	−12.2	6.97	446	0.34	67
LVJ1243+4127	124355.7	+412725	6.09	h	−11.8	7.02	402	1.38	83
KK160	124357.4	+433941	4.33	$TRGB$	−10.9	6.60	293	0.59	47
KKH86	135433.6	+041435	2.61	$TRGB$	−10.3	5.92	287	0.85	51
LeG18	104653.3	+124440	10.40	mem	−11.3	7.15	636	0.28	47
KDG90	121457.9	+361308	2.98	$TRGB$	−11.6	7.66	280	1.55	33
LVJ1217+4703	121710.1	+470349	7.80	mem	−11.0	7.38	394	0.30	46
KK138	122158.4	+281434	6.30	mem	−10.4	6.81	449	0.42	64
KK191	131339.7	+420239	8.28	$TRGB$	−11.4	7.59	371	0.42	18

Table 2. Observation details

Galaxy name	Date of observations	velocity coverage (km s^{-1})	Time on source (Hr)	Synthesized beam (arcsec^2)	Single channel rms (mJy/beam)
(1)	(2)	(3)	(4)	(5)	(6)
AGC112521	December 10, 2010	$-145-734$	6	40.64×35.75, 27.85×22.56, 13.91×10.55	2.0, 1.5, 1.3
KK15	November 14, 2010	$5-886$	4	44.28×36.50, 27.35×24.03, 15.02×11.39	1.4, 1.1, 0.9
KKH37	December 29, 2010	$-643-234$	5.3	54.40×35.55, 25.98×19.19, 12.14×9.85	3.5, 2.6, 1.6
KKH46	December 10, 2010	$251-1133$	3.8	43.26×36.75, 30.03×25.91, 26.54×10.51	3.0, 2.7, 2.0
UGC4879	August 06, 2010	$-154-56$	3.8	48.16×34.03, 34.18×21.52, 25.02×14.78	3.8, 3.2, 2.8
LeG06	October 15, 2010	$831-1272$	6.8	45.00×38.07, 26.95×22.50, 12.40×10.71	3.8, 3.0, 1.1
KDG073	March 14, 2009	$-19-191$	6.75	45.32×35.45, 28.42×22.00, 14.44×10.60	2.8, 1.7, 1.5
VCC0381	August 08, 2010	$273-714$	4.5	45.28×35.57, 31.87×23.50, 23.40×10.27	3.1, 2.9, 2.5
KK141	November 14, 2010	$37-919$	4.5	44.49×35.97, 30.14×24.39, 13.31×9.38	2.1, 1.8, 1.5
KK152	August 09, 2010	$494-1377$	4.5	44.21×33.60, 29.53×21.46, 16.15×9.71	3.7, 3.2, 2.5
UGCA292	December 10, 2010	$-171-708$	4.5	45.22×35.23, 27.79×23.95, 15.09×11.84	2.6, 2.5, 1.9
BTS146	December 11, 2010	$39-920$	5.25	44.28×34.73, 30.92×21.58, 16.29×11.23	1.1, 0.8, 0.7
LVJ1243+4127	January 02, 2011	$-69-811$	3.75	49.86×35.72, 26.71×20.43, 13.92×10.12	3.2, 2.6, 2.0
KK160	December 31, 2010	$-104-775$	4.4	49.27×35.55, 28.43×21.65, 14.01×9.93	2.9, 2.3, 1.5
KKH86	November 13, 2008	$181-392$	5.25	43.20×35.01, 34.17×23.83, 29.53×14.45	2.6, 2.3, 1.8
LeG18	December 11, 2010	$466-1350$	3.75	87.52×35.10, 73.18×23.85, 62.30×9.21	7.4, 9.0, 6.3
PGC1424345	August 12, 2010	$623-1064$	4.5	70.04×33.61, 59.18×20.04, 46.17×16.54	7.5, 8.3, 20.5
KDG090	March 14, 2009	$155-366$	3.3	70.04×33.61, 59.18×20.04, 46.17×16.54	6.3, 4.1, 2.9
LVJ1217+4703	August 07, 2010	$183-623$	4.4	49.20×37.41, 47.16×35.0, 44.06×33.61	4.7, 7.7, 12.1
KK138	December 31, 2010	$39-920$	4.5	42.10×40.14, 27.50×23.83, 11.91×9.51	1.8, 1.7, 1.7
KK191	August 13, 2010	$3-884$	4.5	56.76×34.50, 46.54×18.22, 33.38×11.72	4.9, 4.3, 6.6

vation, with the actual on-source time varying between $\sim$ 2-5 hrs. All data were reduced in classic AIPS. For every galaxy, phase and bandpass calibration was done after editing bad visibilities. Online doppler tracking was not done during observation, hence the data were corrected for earth's motion using AIPS task CVEL. The GMRT has a hybrid configuration (Swarup et al. 1991) with 12 antennas inside the central square (2 km $\times$ 2 km) and 18 antennas spread over $\sim$ 25 km area in an approximate "Y" shaped array. Due to its hybrid configuration, GMRT is capable of sampling both the small and large angular scales within a single observing run. The longest achievable baseline at 21cm wavelength is $\sim$ 120 kλ.

Dirty image cubes at different resolutions were made using the task IMAGR in AIPS by using *'Natural'* and *'Robust'* weighting schemes with different values of uvrange and uvtaper. While the *'Natural'* weighting maximizes the signal to noise ratio, it is know to produce non-gaussian beam profiles and induces complex noise

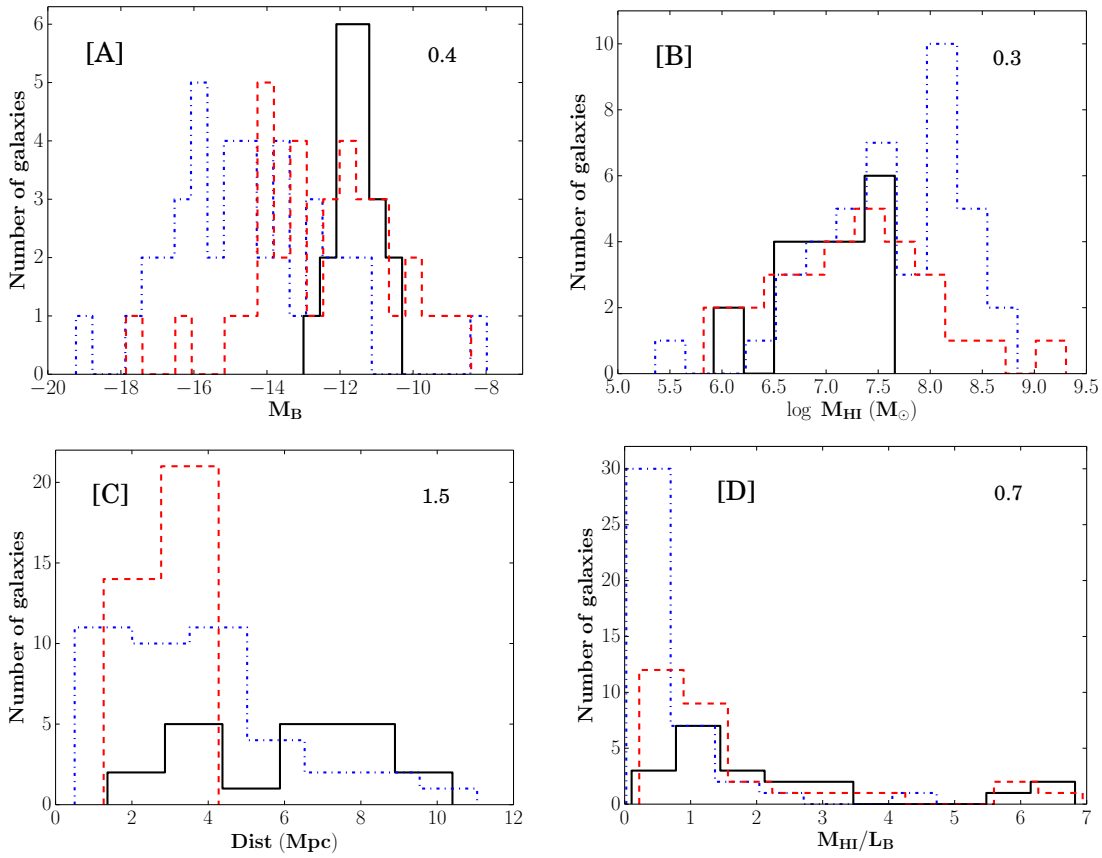

Figure 1. Histograms of different global properties of our sample galaxies. The solid black histograms represent FIGGS2 data (taken form Tab. 1). For comparison we also plot data from two major surveys of dwarf galaxies, namely, the VLA-ANGST and the LITTLE-THINGS survey. The blue dashed-dotted histograms represent data from the LITTLE-THINGS survey whereas the red dashed histograms are for VLA-ANGST survey. For consistency we have kept the bin width of the histograms same for all three surveys. The bin widths are quoted at the top right corners of the respective panels. Panel [A] shows the histograms of extinction corrected absolute blue magnitude (M_B), panel [B] represents the histograms of log of HI mass, panel [C] shows the histograms of distances and in panel [D] we show the histograms of the HI mass to blue luminosity ratio (M_{HI}/L_B).

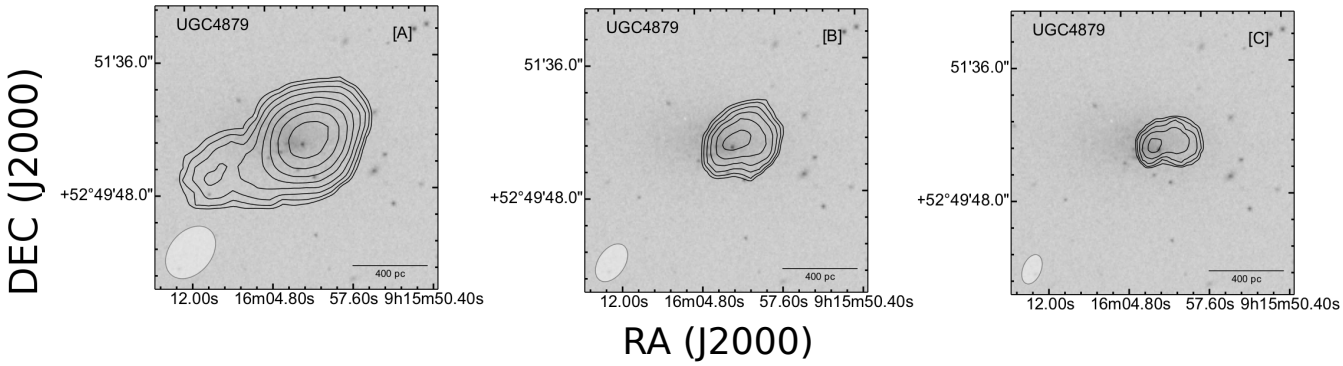

Figure 2. Integrated HI emission from UGC 4879 (contours) at different spatial resolutions overlayed on a DSS B band image (greyscales). The resolution of the images are $48'' \times 34''$ (panel [A]), $34'' \times 21''$ (panel [B]), $25'' \times 14''$ (panel [C]). The contour levels are (1, 1.4, 2, 2.8, ..) 2×10^{19} in panel [A], (1, 1.4, 2, 2.8, ..) 6×10^{19} in panel [B] and (1, 1.4, 2, 2.8, ..) 1×10^{20} in panel [C].

properties into the image. Whereas, *'Robust'* weighting scheme produces somewhat better behaving beam profiles with a diminished SNR. As FIGGS2 sample galaxies are ultra-faint, and a high SNR map favours manual inspection/investigation, we show only *'Natural'* weighted maps in further analysis, though we produced maps using both the weighting schemes. The low resolution dirty cubes were inspected to identify the channels containing HI emission. Since the emission is faint, we found it very difficult and subjective to generate masks for cleaning or generating moment maps. Prior to this we used the line-free channels (identified in the low

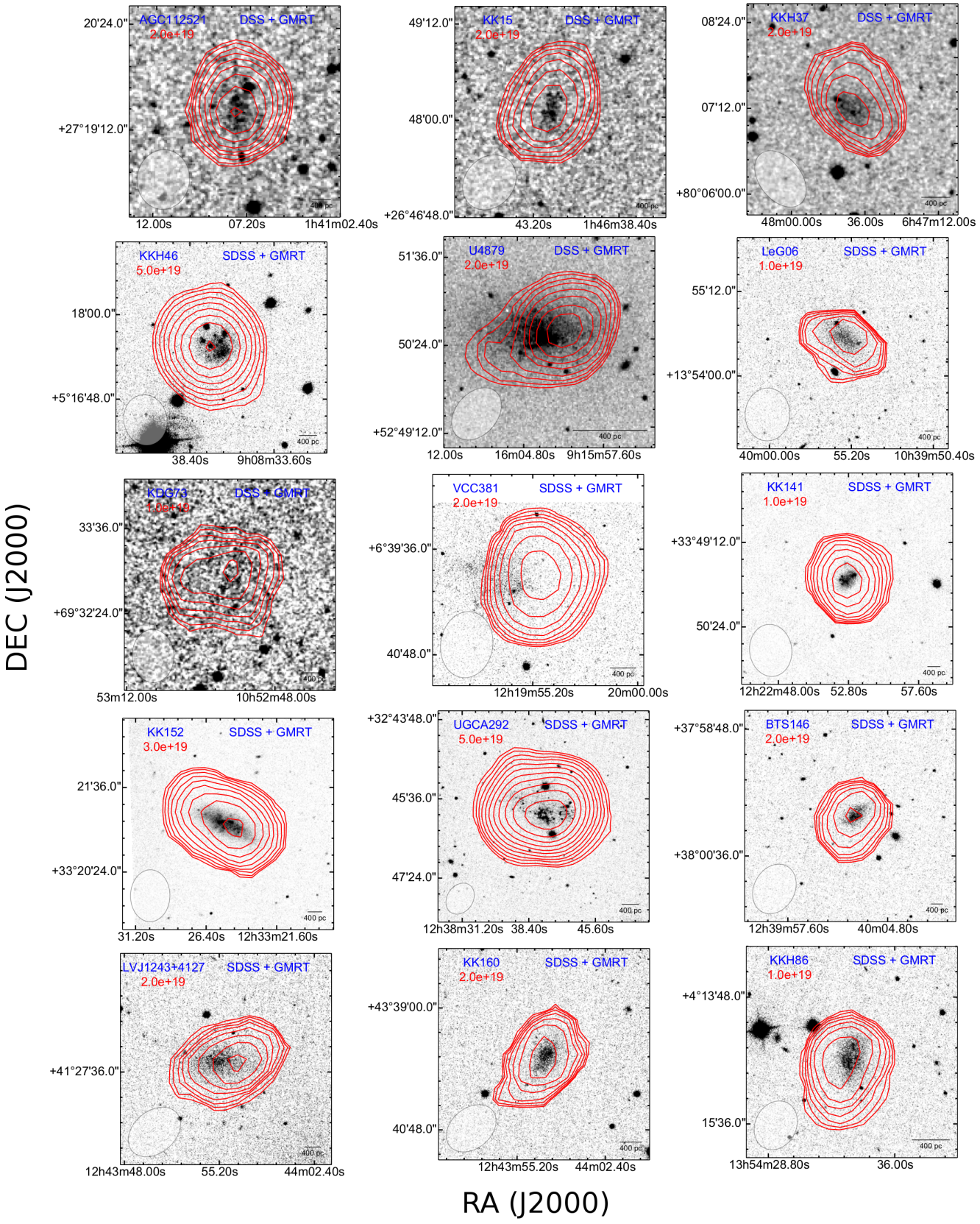

Figure 3. Overlays of the integrated HI emission (contours) on the optical image for the FIGGS2 galaxies. The optical images were taken from SDSS (Abazajian et al. 2009) ('g' filter; λ centred at $\sim$ 4770Å) if available, else DSS images (red filter λ at $\sim$ 6450 Å) were used. The lowest HI contour levels are quoted on the top left of the respective panels in the units of $\mathrm{atoms\ cm^{-2}}$. The successive contours are separated by a factor of $\sqrt{2}$.

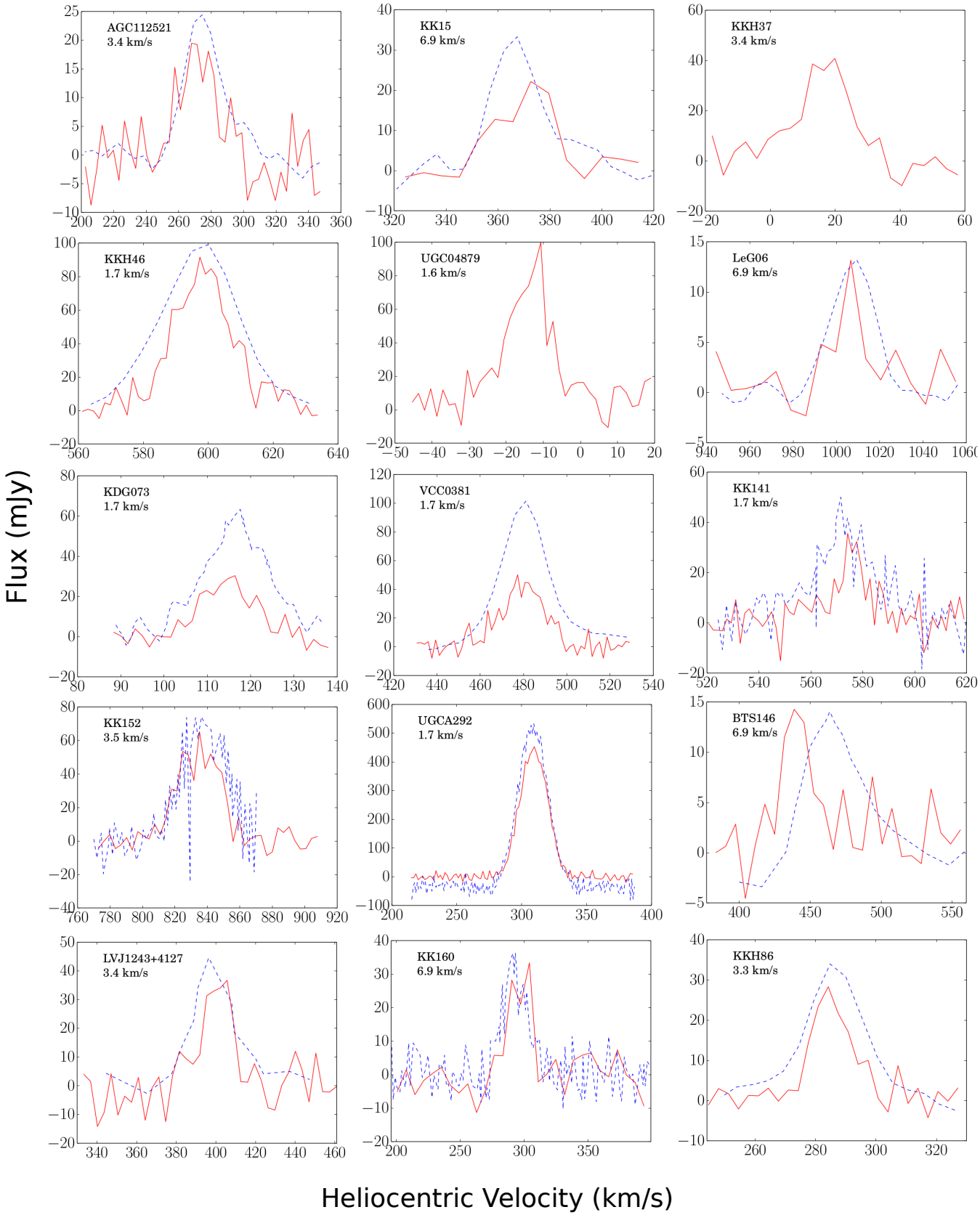

Figure 4. Global HI spectra of our sample galaxies (red solid line) plotted along with the single-dish spectra (blue dashed line). To increase the SNR, multiple channels were collapsed together wherever necessary. The velocity resolution used is quoted in the respective panels. We note that in most of the cases, GMRT observation recovers less flux as compared to single-dish flux. The single-dish spectra for KKH37 and UGC04879 is not available in literature.

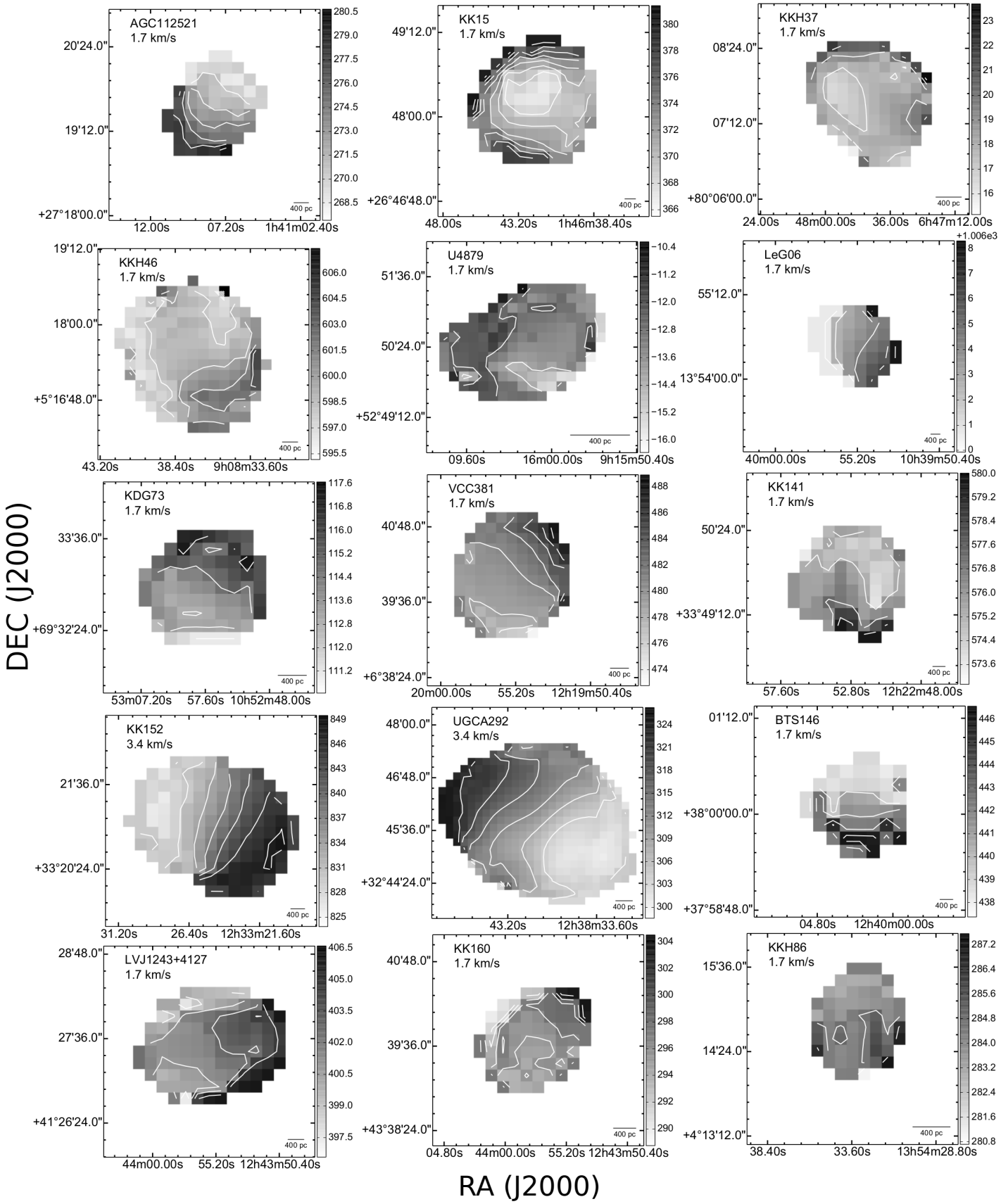

Figure 5. Velocity field of our detected galaxies. The spacing between subsequent contours were quoted at the upper left corner of every panel. Almost all our sample galaxies show ordered rotation in their velocity map.

resolution cube) to fit and subtract the continuum in the image plane using the task IMLIN in AIPS. The continuum subtracted cubes were then cleaned up to an rms level of ~ 2.5 times single channel rms (line free) using the task APCLN. We also tried a multi-scale cleaning but this did not significantly improve the quality of images. Although all of our observations were carried out with a velocity resolution of ~ 1.65 km s^{-1}, we collapsed adjacent channels (reducing velocity resolution) to increase SNR wherever necessary.

Moment maps were made using the task MOMNT in classic AIPS. We smoothed the data using a Gaussian kernel of width 6 pixels in spatial coordinates and a Hanning smoothing of width 3 pixels were applied to the velocity coordinates. We apply a cut off of 1.5-2 times the per channel rms to select emission regions to be included in the moment maps. Total intensity images at different resolutions provide complementary information. For example the effect of local processes like star formation, feedback etc. are best studied using high resolution images, whereas the large-scale dynamics, global extent of HI , dark matter halo properties etc. are better studied using low resolution images. As an example, in Figure 2 we show integrated HI emission images of one of the FIGGS2 sample galaxies, (viz. UGC 4879) at different spatial resolutions. The galaxy shows a faint extended structure at the south-east corner in low resolution image (panel [A]) which is resolved out at higher resolution. On the other hand, the fine details of the morphology of the galaxy in the central region can be more clearly seen in the high resolution images.

We detected HI emission in 15 out of 20 galaxies. Two (LeG18, LVJ1217+4703) out of the five non-detections have quite large single-dish peak fluxes ($>$ 25 mJy (Huchtmeier et al. 2009)). However their GMRT observations were affected by strong RFI and a significant fraction of the data had to be flagged, resulting in higher noise levels in the data cube. Despite the increased noise level, one would have expected to detect the HI emissions at least at 3σ level, and hence the non detections are surprising, if the single dish fluxes are correct. The reason for this discrepancy is unclear to us. Though the quoted single dish flux of KDG90 is quite high ($\sim$ 23.6 Jykm s^{-1}(Koribalski et al. 2004)), this dSph galaxy resides within $\sim 10'$ of the bright spiral NGC4214 having HI flux of 147 Jykm s^{-1}and Holmberg diameter of 8.5 arcmin. Hence, most likely this is a case of HI confusion under single-dish observation. Subsequently, VLA observations (VLA-ANGST survey, (Ott et al. 2012)) also did not detect any emission from this galaxy. The single dish HI spectra for KK138 has a velocity width of 186 km s^{-1} and a very low peak flux of $\sim$10 mJy. Such a large velocity width is not expected for dwarf galaxy; it seems likely that the single dish detection is spurious. In the case of KK191 there is a large spiral galaxy NGC5055 within an angular distance of $\sim 25'$. NGC5055 has a central velocity of 510 km s^{-1} and a velocity width of $\sim$ 400 km s^{-1} which overlaps with the quoted velocity for KK191, i.e. 368 km s^{-1}(Huchtmeier et al. 2000). Hence it is possible that the single dish detection is confused. The observation details and analysis results are presented in Table 2. The columns are as follows: column (1): the galaxy name, column (2): date of observation, column (3): the velocity (heliocentric) coverage of the observing band, column (4): on-source time in hour, column (5): synthesized beam size at different resolution data cubes, column (6): corresponding single channel rms.

In Fig. 4 we overplot the HI global spectra extracted from our observations (red solid lines) on top of the single dish spectra (blue dashed line) (wherever available, see § 5 for more details) of our detected galaxies. From the Figure, it can be seen that almost in all the cases, our observed spectra recovers less flux as compared to the single-dish flux. For example, the synthesis observation of UGC04879 using WSRT (Bellazzini et al. 2011) recovers much more HI flux (2.2$\pm$0.1 Jykm s^{-1}) than what is recovered by the GMRT (1.35$\pm$0.7 Jykm s^{-1}). We expect that this is because the GMRT has fewer short spacings than the WSRT and resolves out most of the low column density extended emission. We have carefully checked our calibration solutions and compared the recovered secondary calibrator fluxes with VLA calibrator manual. In all the cases our fluxes match the catalog value within 10%. A 10% error in calibration is insufficient to explain the flux discrepancies between GMRT spectra and the single-dish spectra.

5 RESULTS & DISCUSSION

In Figure 3 we show the integrated HI distribution (contours) overlayed on the optical images for the detected galaxies. The lowest contour levels are quoted at the upper left corners of each panel in the unit of $\mathrm{atoms\ cm^{-2}}$. We used optical images from SDSS survey ('g' band) whenever available or else we use images from DSS survey ('B' band). We quote the source of the optical images at the top right corner of each panel. To compare the HI and optical extents and to show large scale HI structures of our sample galaxies, we choose to overlay low resolution (higher SNR) HI maps on top of the optical images in Fig. 3. However, due to non-uniform sampling of the visibility plane across our sample, the synthesised beams vary considerably for galaxy to galaxy even after setting the same maximum range of visibility (5 kilo λ) during imaging. The synthesised beams are shown at the left bottom corner of every panel. We note that the optical center and the HI center of many galaxies do not coincide (e.g U4879, KKH86, LVJ1243+4127). We speculate that feedback from star formation could be a possible cause of these offsets.

In Figure 4 we plot the HI global spectra of our detected galaxies (red solid line). As the detected galaxies are very faint, the global spectra at $\sim$ 1.8 km s^{-1} resolution some times has a very low SNR. Hence adjacent channels were collapsed together to increase SNR wherever necessary. The velocity resolutions used for different galaxies are quoted at the upper left corner of the respective panels in Figure 4. We also over-plot the single-dish spectra (blue dashed line) for comparison. For KKH37 and UGC04879 we could not find single dish spectra from literature. For BTS146, we note that there is a difference in the central heliocentric velocity (V_{sys}) between single dish spectra and the GMRT spectra. However, Kovač et al. (2009) observed the same galaxy using WSRT and found a central velocity of 446 $\pm$ 17 km s^{-1}which matches well what we found ($\sim$ 440 km s^{-1}).

The parameters derived from the global spectra are listed in Table 3. The columns are as follows: column (1) the galaxy name, column (2) The integrated HI flux, column (3) systematic velocity (V_{sys}), column (4) the velocity width at 50 percent of the peak flux (Δ_{50}), column (5) The HI diameter derived by ellipse fitting at a column density, $\mathrm{N_{HI}} = 0.3\ \mathrm{M_\odot/pc^2}$, column (6) the ratio of the HI diameter to the optical diameter, column (7) the derived HI mass, column (8) mass to light ratio (M_{HI}/L_B), column (9) the ratio of GMRT flux to single-dish flux, column (10) HI inclination assuming an intrinsic thickness of 0.6 (Roychowdhury et al. 2010). The associated errors are quoted along with the derived parameters. The V_{sys} and the Δ_{50} were derived by fitting a Gaussian profile to the global HI spectra. The quoted errors on V_{sys} and Δ_{50} represent fitting errors only. We estimate the HI diameter by fitting an ellipse to the iso-HI column density contour at

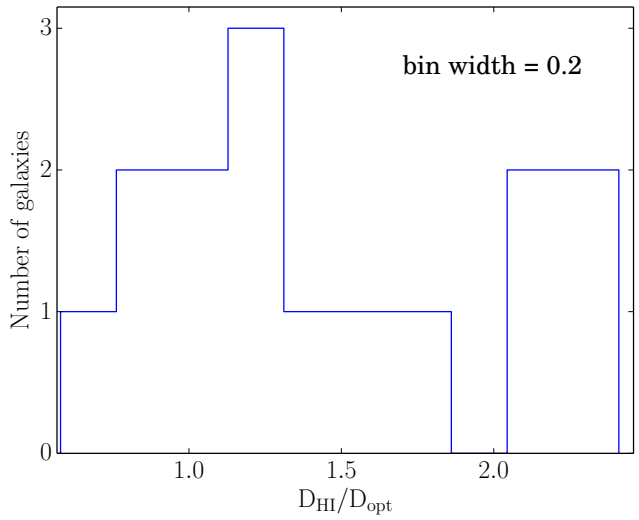

Figure 6. Histogram of HI diameters of our sample galaxies normalized to optical diameter. One can see that almost all our galaxies have HI diameter larger than the optical diameter except one (UGC4879). See the text for more discussion.

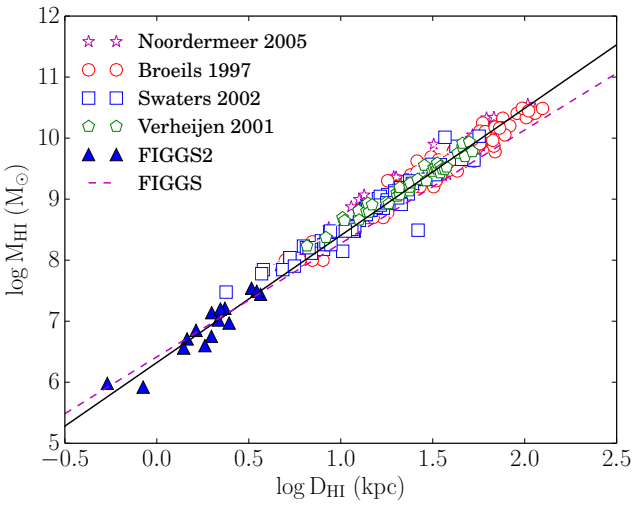

Figure 7. The HI mass (single-dish) of the FIGGS2 sample as a function of HI diameter (measured at a column density of 0.3 $M_\odot pc^{-2}$ (3.75×10^{19} atoms cm^{-2})). The black solid line represents a straight line fit to the FIGGS2 data whereas the magenta dashed line represents a fit to the FIGGS data taken from (Begum et al. 2008). The empty symbols in the plot represent data for spiral galaxies taken from literature. As the large spiral galaxies are bright in HI the D_{HI} for them is defined at a column density of 1 $M_\odot pc^{-2}$ (1.25×10^{20} atoms cm^{-2}).

$N_{HI} = 0.3\ M_\odot/pc^2$. The errors in the estimation of HI diameter (D_{HI}) is expected to be dominated by the errors in the HI map. To account this, we first compute an error map by using the knowledge of the rms in the HI cube and the number of channels used to make the HI map. We then estimate a typical error involved in measured column density at $N_{HI} = 0.3\ M_\odot/pc^2$ contours (i.e. the mean error along the $N_{HI} = 0.3\ M_\odot/pc^2$ contour from the error map). We then construct 1000 realization of N_{HI} which are consistent with $N_{HI} = 0.3\ M_\odot/pc^2$ within the error. We use these N_{HI} values for HI isophotes and fit ellipses to these isophotes. We use the standard deviation as an estimate of the errors in the fit parameters. The errors in D_{HI}, D_{HI}/D_{opt} and i_{HI} were estimated in this way.

In Figure 5 we present the velocity fields of the detected galaxies. We note that in many cases emission has been detected only across a few channels. As the SNR is poor, we did not take a Gaussian-Hermite polynomial fitting approach to derive the velocity field. Instead we adopted the intensity weighted first moment of the spectral cube as the velocity field. From Figure 5, we can see that, there are ordered velocity fields which is an indication of rotation in many galaxies (e.g. AGC112521, LeG06, KDG73, VCC381). But at the same time there are a few galaxies in the sample which show chaotic velocity fields, for example, KKH86, KK160, KKH37. The chaotic appearance of the velocity field could be due to the low SNR and low spatial resolution in the spectral cube. For the same reasons, the PV diagrams are noisy and do not bring out kinematics of the galaxies and hence we do not present them here.

In Figure 6 we plot the histogram of HI diameters of our sample galaxies. To compare the extent of HI disks with their optical counterparts, we normalised the HI diameter by the optical diameter (D_{opt}) of the galaxies. Isophotal radii e.g. R_{Holm} or R_{25} have limited meaning for dwarf galaxies having low surface brightness. These radii estimates could be prone to systematic under-estimation of their optical extent. Hence we perform photometric analysis of B-band image of our galaxies, and fit the surface brightness profiles with an exponential profile. Adopting a convention by (Swaters et al. 2002), we define optical radii as 3.2 times exponential scale length. However for four of our detected galaxies (KKH37, LeG06, KDG073 and KKH86), optical photometry (in B band) could not be performed due to poor quality of available data. For these galaxies, we considered Holmberg radius as optical radii. In many previous HI surveys (Broeils and Rhee 1997; Verheijen and Sancisi 2001a; Swaters et al. 2002; Noordermeer et al. 2005) an isophote of 1 $M_\odot pc^{-2}$ was adopted for ellipse fitting and estimating the HI radii. However, most of our detected galaxies, fall short of HI surface density of 1 $M_\odot pc^{-2}$ even at the center. We have used an face-on HI surface density of 0.3 $M_\odot pc^{-2}$ (3.75×10^{19} atoms cm^{-2}) isophote to estimate the HI diameter. The mean value of normalised HI diameter is 1.54 which is somewhat lower than the value found for the FIGGS (Begum et al. 2008) sample which is 2.40. This may be in part to the very faint outer emission being resolved out. From our data, we found that for all our sample galaxies, HI disk extends more than the optical disk except one. For the galaxy UGC4879, the HI disk found to be smaller than its optical counterpart. From Figure 3 (5th image) we note that, a faint extended HI emission is seen in the south-east corner, which may be indicative of diffuse emission not picked up in our observations. It is worth noting that for UGC04879 the GMRT observation picks up only about 50% of the single dish flux.

The HI diameter and the HI mass of different types of galaxies exhibits a tight correlation. In Figure 7 we plot the correlation between the HI diameter and the HI mass of our sample galaxies (filled blue triangles). As the GMRT resolves out a significant amount of HI at low column densities at the outer radii (as noted in §4), we use single-dish HI flux measurements in Fig. 7. To compare the correlation with larger galaxies, we over plot data for spiral galaxies (HI diameter defined at an HI surface density of 1 $M_\odot pc^{-2}$) from various previous HI surveys (Broeils and Rhee 1997; Verheijen and Sancisi 2001a; Swaters et al. 2002; Noordermeer et al. 2005). The solid black line represents a linear fit to our (FIGGS2) data whereas the dashed magenta line represents a lin-

Table 3. Results from the GMRT observations of FIGGS2 sample galaxies

Galaxy	FI_{GMRT} (Jy km s^{-1})	V_{sys} (km s^{-1})	ΔV_{50} (km s^{-1})	D_{HI} (arcmin)	D_{HI}/D_{opt}	M_{HI} ($\times 10^7$ $M_\odot$)	M_{HI}/L_B	FI_{GMRT}/FI_{SD}	i_{HI} (^{o})
(1)	(2)	(3)	(4)	(5)	(6)	(7)	(8)	(9)	(10)
AGC112521	0.44 ± 0.34	270.4 ± 0.2	25.0 ± 3.8	1.12 ± 0.14	1.9 ± 0.2	0.38 ± 0.29	0.67 ± 0.51	0.7 ± 0.5	44 ± 7
KK15	0.52 ± 0.19	371.3 ± 1.3	23.8 ± 3.1	0.93 ± 0.14	1.6 ± 0.2	0.92 ± 0.34	1.12 ± 0.42	0.6 ± 0.2	63 ± 6
KKH37	0.70 ± 0.13	17.4 ± 0.1	17.2 ± 0.9	1.46 ± 0.12	1.3 ± 0.1	0.20 ± 0.04	0.29 ± 0.05	0.4 ± 0.1	64 ± 4
KKH46	1.96 ± 0.47	598.2 ± 0.3	21.2 ± 0.8	1.88 ± 0.23	3.1 ± 0.4	2.07 ± 0.49	1.59 ± 0.38	0.8 ± 0.2	39 ± 4
UGC04879	1.35 ± 0.66	-13.2 ± 0.2	14.2 ± 1.2	1.36 ± 0.37	0.4 ± 0.1	0.06 ± 0.03	0.06 ± 0.03	0.5 ± 0.3	46 ± 7
LeG06	0.22 ± 0.37	1005.9 ± 2.6	16.3 ± 6.6	0.54 ± 0.31	0.9 ± 0.5	0.56 ± 0.94	0.62 ± 1.04	0.8 ± 1.3	54 ± 17
KDG073	0.40 ± 0.18	114.6 ± 0.5	14.2 ± 1.2	1.23 ± 0.30	1.0 ± 0.2	0.13 ± 0.06	0.39 ± 0.18	0.4 ± 0.2	71 ± 14
VCC0381	1.07 ± 0.30	479.8 ± 0.2	22.9 ± 1.3	1.45 ± 0.11	1.9 ± 0.1	0.56 ± 0.16	0.74 ± 0.21	0.4 ± 0.1	38 ± 5
KK141	0.43 ± 0.18	576.0 ± 0.8	14.5 ± 1.8	0.98 ± 0.19	2.4 ± 0.5	0.61 ± 0.26	0.98 ± 0.41	0.4 ± 0.2	45 ± 11
KK152	1.78 ± 0.37	834.7 ± 0.9	30.5 ± 2.0	1.63 ± 0.18	1.5 ± 0.2	2.00 ± 0.42	0.80 ± 0.17	0.6 ± 0.1	66 ± 4
UGCA292	11.67 ± 0.62	309.2 ± 0.1	24.6 ± 0.3	3.12 ± 0.22	3.1 ± 0.2	4.08 ± 0.22	4.51 ± 0.24	1.3 ± 0.1	37 ± 4
BTS146	0.39 ± 0.15	440.5 ± 1.8	25.5 ± 4.3	1.00 ± 0.15	2.9 ± 0.4	0.66 ± 0.26	0.56 ± 0.22	0.7 ± 0.3	59 ± 7
LVJ1243+4127	0.62 ± 0.53	403.2 ± 0.0	16.5 ± 2.6	1.22 ± 0.20	0.9 ± 0.1	0.54 ± 0.46	0.66 ± 0.56	0.5 ± 0.4	68 ± 5
KK160	0.51 ± 0.53	301.6 ± 0.1	20.0 ± 3.4	1.45 ± 0.31	2.5 ± 0.5	0.22 ± 0.23	0.62 ± 0.65	0.6 ± 0.6	71 ± 8
KKH86	0.45 ± 0.16	285.0 ± 0.7	15.1 ± 1.5	1.11 ± 0.22	1.3 ± 0.3	0.07 ± 0.03	0.35 ± 0.13	0.9 ± 0.3	59 ± 9

ear fit for FIGGS survey. It can be seen that due to the small size of our sample galaxies, our study extended this correlation to low mass and low diameter end. From the figure it can be noted that our data points follow the trend for spiral galaxies (hollow points) or for the FIGGS galaxies (magenta dashed line). However, we note that our data points might be affected by the facts that the D_{HI} were measured at a different HI column density for FIGGS2 and for the spiral galaxies.

The best linear fit of D_{HI} vs M_{HI} correlation (black solid line) could be represented by

$$\log(M_{HI}) = (2.08 \pm 0.20)\log(D_{HI}) + (6.32 \pm 0.07) \quad (1)$$

In Fig.7 the dashed magenta line represents the correlation for FIGGS galaxies. The slope and the intercept for FIGGS2 galaxies (i.e. 2.08 ± 0.20 and 6.32 ± 0.07) roughly matches with that of the FIGGS galaxies.

In Figure 8 we show the $\log(M_{HI}/L_B)$ as a function of M_B. Our sample galaxies are shown by filled (GMRT HI mass) and hollow (Single dish HI mass) blue triangles, whereas the red hollow asterisks represent the FIGGS sample. The blue hollow squares are from Warren et al. (2007) and green hollow pentagons are for galaxies from Verheijen and Sancisi (2001b). The solid line represents an empirically derived upper limit to the (M_{HI}/L_B) from Warren et al. (2007). It can be thought of as a minimum fraction of the baryonic mass to be converted into stars in order to be stable under thermal equilibrium with gravity (Warren et al. 2007) for a galaxy of given baryonic mass. It is interesting to note that all our sample galaxies lies well below the solid line (even with single-dish HI mass). It implies that these small dwarf galaxies converted much more gas into stars than the minimum required to be stable under the balance of gravity and thermal energy.

In summary we have observed 20 faint galaxies with the GMRT to extend the FIGGS sample towards the low luminosity end. We detected HI emission from 15 of the galaxies. We find that these galaxies have the similar HI mass to HI diameter relation as the brighter dwarfs. These data will be useful for a host of studies of dwarf galaxies, including the interplay between gas and star formation, the phase structure of the atomic ISM, the structure and distribution of the dark matter halos, etc.

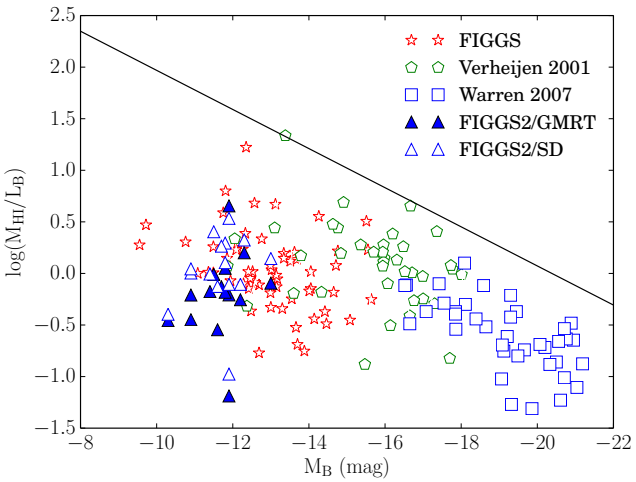

Figure 8. The log of HI -mass-to-light ratio as a function of M_B. Blue filled (GMRT HI mass) and hollow (Single dish HI mass) triangles are from FIGGS2, red hollow asterisks represent data from FIGGS survey whereas blue hollow squares and green hollow pentagons represent Warren et al. (2007) and Verheijen and Sancisi (2001b) respectively. The solid line represents an empirically derived upper limit to M_{HI}/L_B from (Warren et al. 2007). See text for more details.

6 ACKNOWLEDGEMENTS

NNP would like to thank the anonymous referee for her/his valuable comments which helped to improve the paper significantly. NNP would like to thank the GMRT staff members for making the observations possible. The Giant Meter-wave Radio Telescope is run by the National Centre for Radio Astrophysics of the Tata Institute of Fundamental Research. IDK & MES thanks for the support from Russian Foundation for Basic Research, grant 15-52-45004, and the Russian Science Foundation, grant 14-02-00965.

REFERENCES

Abazajian, K. N., Adelman-McCarthy, J. K., Agüeros, M. A., Al-

lam, S. S., Allende Prieto, C., An, D., Anderson, K. S. J., Anderson, S. F., Annis, J., Bahcall, N. A., and et al. (2009). The Seventh Data Release of the Sloan Digital Sky Survey. *ApJS*, 182:543–558.

Banerjee, A. and Jog, C. J. (2008). The Flattened Dark Matter Halo of M31 as Deduced from the Observed H I Scale Heights. *ApJ*, 685:254–260.

Banerjee, A., Matthews, L. D., and Jog, C. J. (2010). Dark matter dominance at all radii in the superthin galaxy UGC 7321. *NewA*, 15:89–95.

Banerjee, A., Patra, N. N., Chengalur, J. N., and Begum, A. (2013). A slow bar in the dwarf irregular galaxy NGC 3741. *MNRAS*, 434:1257–1263.

Begum, A., Chengalur, J. N., Karachentsev, I. D., Sharina, M. E., and Kaisin, S. S. (2008). FIGGS: Faint Irregular Galaxies GMRT Survey - overview, observations and first results. *MNRAS*, 386:1667–1682.

Bellazzini, M., Beccari, G., Oosterloo, T. A., Galleti, S., Sollima, A., Correnti, M., Testa, V., Mayer, L., Cignoni, M., Fraternali, F., and Gallozzi, S. (2011). An optical and H i study of the dwarf Local Group galaxy VV124 = UGC4879. A gas-poor dwarf with a stellar disk? *A&A*, 527:A58.

Broeils, A. H. and Rhee, M.-H. (1997). Short 21-cm WSRT observations of spiral and irregular galaxies. HI properties. *A&A*, 324:877–887.

Cannon, J. M., Giovanelli, R., Haynes, M. P., Janowiecki, S., Parker, A., Salzer, J. J., Adams, E. A. K., Engstrom, E., Huang, S., McQuinn, K. B. W., Ott, J., Saintonge, A., Skillman, E. D., Allan, J., Erny, G., Fliss, P., and Smith, A. (2011). The Survey of H I in Extremely Low-mass Dwarfs (SHIELD). *ApJL*, 739:L22.

Giovanelli, R., Haynes, M. P., Kent, B. R., Perillat, P., Saintonge, A., Brosch, N., Catinella, B., Hoffman, G. L., Stierwalt, S., Spekkens, K., Lerner, M. S., Masters, K. L., Momjian, E., Rosenberg, J. L., Springob, C. M., Boselli, A., Charmandaris, V., Darling, J. K., Davies, J., Garcia Lambas, D., Gavazzi, G., Giovanardi, C., Hardy, E., Hunt, L. K., Iovino, A., Karachentsev, I. D., Karachentseva, V. E., Koopmann, R. A., Marinoni, C., Minchin, R., Muller, E., Putman, M., Pantoja, C., Salzer, J. J., Scodeggio, M., Skillman, E., Solanes, J. M., Valotto, C., van Driel, W., and van Zee, L. (2005). The Arecibo Legacy Fast ALFA Survey. I. Science Goals, Survey Design, and Strategy. *AJ*, 130:2598–2612.

Huchtmeier, W. K., Karachentsev, I. D., and Karachentseva, V. E. (2009). HI-observations of dwarf galaxies in the Local Supercluster. *A&A*, 506:677–680.

Huchtmeier, W. K., Karachentsev, I. D., Karachentseva, V. E., and Ehle, M. (2000). HI observations of nearby galaxies . I. The first list of the Karachentsev catalog. *A&AS*, 141:469–490.

Hunter, D. A., Ficut-Vicas, D., Ashley, T., Brinks, E., Cigan, P., Elmegreen, B. G., Heesen, V., Herrmann, K. A., Johnson, M., Oh, S.-H., Rupen, M. P., Schruba, A., Simpson, C. E., Walter, F., Westpfahl, D. J., Young, L. M., and Zhang, H.-X. (2012). Little Things. *AJ*, 144:134.

Karachentsev, I. D., Karachentseva, V. E., and Huchtmeier, W. K. (2001). H I observations of nearby galaxies. III. More dwarf galaxies in the northern sky. *A&A*, 366:428–438.

Karachentsev, I. D., Karachentseva, V. E., Huchtmeier, W. K., and Makarov, D. I. (2004). A Catalog of Neighboring Galaxies. *AJ*, 127:2031–2068.

Karachentsev, I. D., Makarov, D. I., and Kaisina, E. I. (2013). Updated Nearby Galaxy Catalog. *AJ*, 145:101.

Koribalski, B. S., Staveley-Smith, L., Kilborn, V. A., Ryder, S. D., Kraan-Korteweg, R. C., Ryan-Weber, E. V., Ekers, R. D., Jerjen, H., Henning, P. A., Putman, M. E., Zwaan, M. A., de Blok, W. J. G., Calabretta, M. R., Disney, M. J., Minchin, R. F., Bhathal, R., Boyce, P. J., Drinkwater, M. J., Freeman, K. C., Gibson, B. K., Green, A. J., Haynes, R. F., Juraszek, S., Kesteven, M. J., Knezek, P. M., Mader, S., Marquarding, M., Meyer, M., Mould, J. R., Oosterloo, T., O'Brien, J., Price, R. M., Sadler, E. M., Schröder, A., Stewart, I. M., Stootman, F., Waugh, M., Warren, B. E., Webster, R. L., and Wright, A. E. (2004). The 1000 Brightest HIPASS Galaxies: H I Properties. *AJ*, 128:16–46.

Kovač, K., Oosterloo, T. A., and van der Hulst, J. M. (2009). A blind HI survey in the Canes Venatici region. *MNRAS*, 400:743–765.

Makarov, D. I., Karachentsev, I. D., and Burenkov, A. N. (2003). New optical velocities of nearby dwarf LSB galaxies. *A&A*, 405:951–957.

Narayan, C. A. and Jog, C. J. (2002). Origin of radially increasing stellar scaleheight in a galactic disk. *A&A*, 390:L35–L38.

Noordermeer, E., van der Hulst, J. M., Sancisi, R., Swaters, R. A., and van Albada, T. S. (2005). The Westerbork HI survey of spiral and irregular galaxies. III. HI observations of early-type disk galaxies. *A&A*, 442:137–157.

Ott, J., Stilp, A. M., Warren, S. R., Skillman, E. D., Dalcanton, J. J., Walter, F., de Blok, W. J. G., Koribalski, B., and West, A. A. (2012). VLA-ANGST: A High-resolution H I Survey of Nearby Dwarf Galaxies. *AJ*, 144:123.

Patra, N. N., Banerjee, A., Chengalur, J. N., and Begum, A. (2014). Modelling H I distribution and kinematics in the edge-on dwarf irregular galaxy KK250. *MNRAS*, 445:1424–1429.

Patra, N. N., Chengalur, J. N., and Begum, A. (2013). The H I column density distribution function in faint dwarf galaxies. *MNRAS*, 429:1596–1601.

Patra, N. N., Chengalur, J. N., Karachentsev, I. D., Kaisin, S. S., and Begum, A. (2016). Cold H I in faint dwarf galaxies. *MNRAS*, 456:2467–2485.

Roychowdhury, S., Chengalur, J. N., Begum, A., and Karachentsev, I. D. (2009). Star formation in extremely faint dwarf galaxies. *MNRAS*, 397:1435–1453.

Roychowdhury, S., Chengalur, J. N., Begum, A., and Karachentsev, I. D. (2010). Thick gas discs in faint dwarf galaxies. *MNRAS*, 404:L60–L63.

Roychowdhury, S., Chengalur, J. N., Kaisin, S. S., Begum, A., and Karachentsev, I. D. (2011). Small Bites: star formation recipes in extreme dwarfs. *MNRAS*, 414:L55–L59.

Roychowdhury, S., Chengalur, J. N., Karachentsev, I. D., and Kaisina, E. I. (2013). The intrinsic shapes of dwarf irregular galaxies. *MNRAS*, 436:L104–L108.

Saha, K. and Maciejewski, W. (2013). Spontaneous formation of double bars in dark-matter-dominated galaxies. *MNRAS*, 433:L44–L48.

Swarup, G., Ananthakrishnan, S., Kapahi, V. K., Rao, A. P., Subrahmanya, C. R., and Kulkarni, V. K. (1991). The Giant Metre-Wave Radio Telescope. *Current Science, Vol. 60, NO.2/JAN25, P. 95, 1991*, 60:95.

Swaters, R. A., van Albada, T. S., van der Hulst, J. M., and Sancisi, R. (2002). The Westerbork HI survey of spiral and irregular galaxies. I. HI imaging of late-type dwarf galaxies. *A&A*, 390:829–861.

Verheijen, M. A. W. and Sancisi, R. (2001a). The Ursa Major cluster of galaxies. IV. HI synthesis observations. *A&A*, 370:765–867.

Verheijen, M. A. W. and Sancisi, R. (2001b). The Ursa Major cluster of galaxies. IV. HI synthesis observations. *A&A*, 370:765–867.

Warren, B. E., Jerjen, H., and Koribalski, B. S. (2007). The Minimum Amount of Stars a Galaxy Will Form. *AJ*, 134:1849.